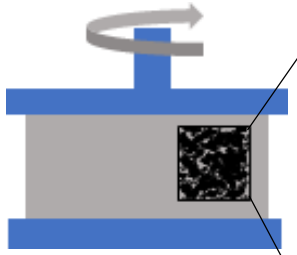

Macroscopic rheological measurements

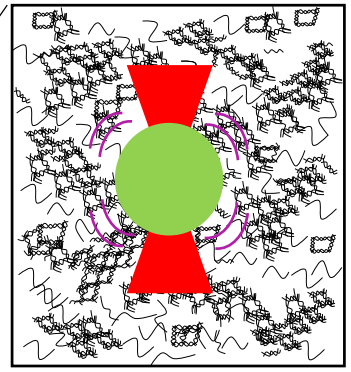

Passive microrheology

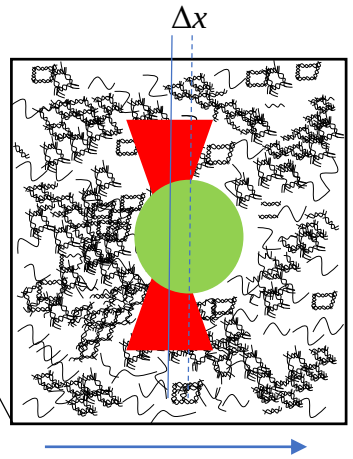

Active microrheology

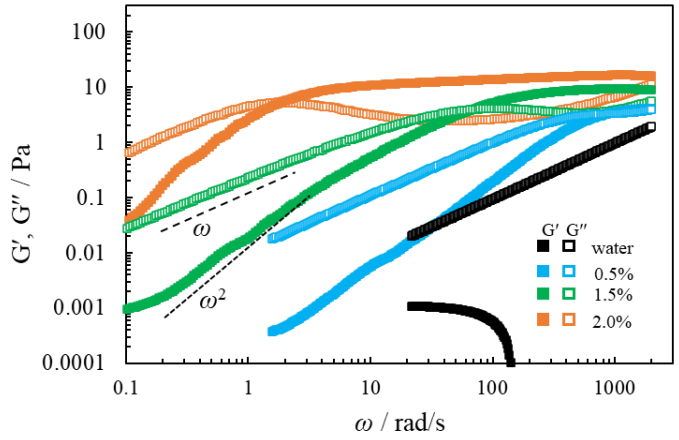

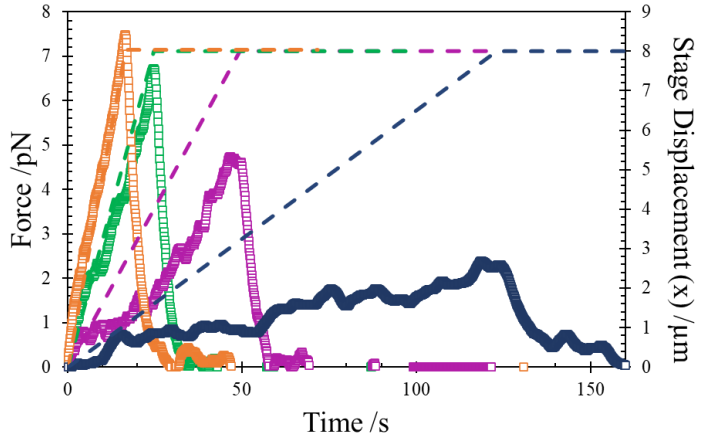

Microrheological properties and local structure of ι-carrageenan gels probed by using optical tweezers

Lester C. Geonzon[1], Motoyoshi Kobayashi[1*], Manlio Tassieri[2], Rommel G. Bacabac[3], Yasuhisa Adachi[1], Shingo Matsukawa[4]

[1] *Faculty of Life and Environmental Sciences, University of Tsukuba, 1-1-1 Tennodai, Tsukuba, Ibaraki, 305-8572, Japan*

[2] *James Watt School of Engineering, University of Glasgow, Glasgow, G12 8LT, United Kingdom*

[3] *Medical Biophysics Group, Department of Physics, University of San Carlos, Cebu City, 6000, Philippines*

[4] *Department of Food Science and Technology, Tokyo University of Marine Science and Technology, 4-5-7 Konan, Minato-ku, Tokyo 108-8477, Japan*

*Corresponding author:

Name: Motoyoshi Kobayashi, Ph.D.

E-mail Address: kobayashi.moto.fp@u.tsukuba.ac.jp

Tel & Fax: +81-(0)29-853-5721

Address: Faculty of Life and Environmental Sciences, University of Tsukuba

1-1-1 Tennodai, Tsukuba, Ibaraki, 305-8572, Japan

Abstract

Iota carrageenan (IC) is one of the most important gelling carrageenans in food and biotechnological applications; however, some of its potential applications have been constrained by its weak gelation ability. In order to better understand the origin of the weak mechanical response of IC gels, the hierarchical network structure based on meso- and microrheological properties of IC gels at 20 °C were probed via passive and active microrheology both performed by using optical tweezers (OT). Passive microrheology captures a wide spectral content of IC viscoelastic properties, revealing a rubbery plateau of the elastic modulus at relatively high frequencies for all IC concentrations; thus, uncovering the dynamics of the network. Moreover, different microstructures of IC gels were inferred by analyzing the concentration-dependent stress response when applying large deformation to the network. At low IC concentration, yielding was observed as indicated by the stress-independent response vs. strain, implying the structural rearrangement and disentanglement. As the IC concentration increased, the yielding diminished with increasing strain rate due to increased entanglement density, which limits the rearrangement of clusters. Therefore, this study presents novel insights into the meso- and microscale properties of IC gels that otherwise would not be accessible by conventional bulk rheology and submicroscopic probe diffusion measurements.

Keywords: Optical tweezers-based microrheology/ carrageenan gel / mesoscale properties/ local large deformation

1. Introduction

Carrageenans are a family of water-soluble, linear sulfated polysaccharides extracted from various species of red algae. It is composed of alternating units of 1,3-linked β-D-galactopyranose (G) and 1,4-linked 3,6-anhydro-α-D- galactopyranose (AG) units. Owed to its nontoxicity and biocompatibility, carrageenans are widely used in the food industry (Mundo, Zhou, Tan, Liu, & McClements, 2021; Roesch, Cox, Compton, Happe, & Corredig, 2004; Simeone, Tassieri, Sibillo, & Guido, 2005); and they have the potential of being used for developing products in medical and biotechnological applications (Bai & Tuvikene, 2021; Barabanova et al., 2008; Cao et al., 2021; Necas & Bartosikova, 2013). In industry, gel-forming carrageenans are the most utilized carrageenan, including κ-carrageenan (KC) and ι-carrageenan (IC). These carrageenans only differ in the degree of sulfation: one (G4S-DA) for KC and two (G4S-DA2S) for IC (Azevedo, Torres, Sousa-Pinto, & Hilliou, 2015; Usov, 1992), which results in a noticeable difference in the gelation properties: i.e., KC forms a brittle and robust gel, whereas IC forms a soft and weak gel (Chronakis, Doubler, & Piculell, 2000; Robal et al., 2017). Still, the weak gel properties of the IC gels limit their potential applications as compared to the hard and brittle KC gels.

The gel formation and network structure of carrageenan have been associated to the conformational changes of the molecules from random coil to helix structure (Rees, Steele, & Williamson, 1969; Rochas, Rinaudo, & Landry, 1989). This conformational transition gives rise to the viscoelastic properties of carrageenan gels, whereas the extensive aggregation of KC helix structures is generally accepted to generate stiff and brittle KC gels (Hu, Du, & Matsukawa, 2016; Liu, Chan, & Li, 2015; Rochas et al., 1989). However, despite

66 the small difference in the molecular structure between KC and IC, an apparent difference
67 in the physical property and gelation mechanism has been realized. Hence, the network
68 structure of IC gels has been the subject of research interest in the past decades. The physical
69 property and network structure formation of IC gels has been investigated using different
70 techniques to elucidate the underlying gelation mechanisms from different perspectives
71 (Geonzon, Descallar, Du, Bacabac, & Matsukawa, 2020). Bulk rheological properties and
72 differential scanning calorimetry (DSC) measurements revealed the gelation of IC gels and
73 suggested that IC formed only a few IC helical aggregates (Chronakis et al., 2000; Du,
74 Brenner, Xie, & Matsukawa, 2016; Takemasa, Chiba, & Date, 2001). On the other hand,
75 several studies utilized imaging techniques to infer the network structure of IC gels using
76 electron microscopy and confocal laser scanning microscopy (Amici, Clark, Normand, &
77 Johnson, 2001; Bui, Nguyen, Nicolai, & Renou, 2019; Thrimawithana, Young, Dunstan, &
78 Alany, 2010). Although the methods provide direct information on the microstructure, the
79 invasive sample treatment may alter the actual gel structure. Furthermore, polymer diffusion
80 measurements using NMR and FRAP have demonstrated the gradual formation of IC
81 aggregates, where some free polymers were not connected to the aggregates (Bui et al., 2019;
82 Zhao & Matsukawa, 2012). Moreover, submicroscopic measurements using particle
83 tracking have suggested the formation of IC aggregates or the loosely connected network of
84 IC chains (Geonzon, Bacabac, & Matsukawa, 2019b). However, the diffusion measurements
85 come with some limitations, as they rely on the thermal fluctuations of the polymers, and
86 therefore the tracer particles cannot probe the materials' response at larger length scales.
87 Thus, the network structure of weak IC gels could not be resolved. Moreover, there exists

a ‘size domain’ (i.e., length scale) that is often overlooked in experimental investigations of IC gels, specifically at meso- and microscopic scales, which are not accessible by conventional bulk and diffusion measurements. Therefore, to gain a full picture of the hierarchical structure of IC gels, it is imperative to shorten further the gap between macroscopic and submicroscopic investigations, as for the aim of this work by utilizing techniques capable of elucidating meso- and microscopic properties.

The optical tweezers (OT) are extremely versatile tools used in a variety of different applications within the Natural Sciences (Ashkin, Dziedzic, & Bjorkholm, 1986; Berg-Sørensen & Flyvbjerg, 2004; Geonzon, Kobayashi, & Adachi, 2021; Geonzon, Kobayashi, Sugimoto, & Adachi, 2022; Svoboda, Schmidt, Schnapp, & Blck, 1993; Tassieri, 2016). Among the many applications, OT have been successfully used in the field of rheology because of its ability to access the local mechanical properties of materials within both the linear and the nonlinear regimes. Linear microrheological measurements can be performed in two modes, either in passive or active microrheology (Mizuno, Head, MacKintosh, & Schmidt, 2008; Shindel & Furst, 2015). The first analyses the thermally driven motion of the probe particles to infer the local rheological properties of the surrounding media by exploiting the generalized Stokes-Einstein relationship (Mason, 2000; Tassieri, 2016; Vyas et al., 2016; Waigh, 2016). The key advantage of passive microrheology over conventional bulk rheology is that it can access a wider frequency spectrum. Additionally, only a few studies use OT to probe the microrheological properties of polysaccharide gels. Del Giudice et al. studied rheology and nonlinear rheology of hydroxyethyl cellulose through different rheological techniques, including OT, to provide new insights into the morphological

structure of HEC molecules. Meanwhile, Tassieri et al. measured the microrheology of glucuronoxylomannan using passive microrheology by OT. Moreover, multiple particle tracking and OT-based microrheology can reveal inherent heterogeneities in the network structure and scale-dependent rheology, which are not accessible by macroscopic measurements (Geonzon et al., 2019a; Hori, Penaloza, Shundo, & Tanaka, 2012; Maki & Annaka, 2020; Van Mameren et al., 2006; Yang, Lv, Jia, Nishinari, & Fang, 2017). Notably, OT-based microrheology can access the materials' nonlinear regimes by driving the probe particles to relatively large deformations (Chapman & Robertson-Anderson, 2014; Falzone, Blair, & Robertson-Anderson, 2015; Gomez-Solano & Bechinger, 2014; Gomez-Solano & Bechinger, 2015; Robertson-Anderson, 2018). This approach can give access to the materials' mechanical properties at large length scales, i.e., within the mesoscale domain, and extract near macroscopic properties (Robertson-Anderson, 2018). Therefore, by using OT to probe the materials' linear and nonlinear regimes, we can address the knowledge gap between the macroscopic and the submicroscopic rheological perspectives of the hierarchical structure of IC gels. Although this is not a direct microstructural analysis, this approach also provided pivotal information on the network structure of IC gels.

In this study, we have adopted optical tweezers to investigate the microscopic wideband viscoelastic properties of IC gels, which have revealed interesting features at relatively high frequencies. Notably, the outcomes have been corroborated by conventional bulk rheology measurements. Moreover, the mesoscopic properties of IC gels were investigated by means of active microrheology measurements, which were achieved by entraining an optically trapped particle with a flow generated by moving the microscope stage. Our collective

results provide new insights into the hierarchical structure of IC gels, as elucidated hereafter.

2. Materials and Methods

2.1 Materials

The ι- carrageenan (IC) powder was purchased from Tokyo Chemical Industry Co., Ltd. (Tokyo, Japan). The IC was dialyzed against ~200 mM NaCl solution and afterward against deionized water. The ion concentrations of the dialyzed samples were measured by inductively coupled plasma atomic emission, wherein 0.63% for Na^+ and 0.11% for K^+, while no Mg^{2+} or Ca^{2+} was detected. The molecular weight, M_w, of dialyzed IC samples was around 360 kDa, obtained via pullulan (Hayashibara Co., Ltd., Japan) converted molecular weight (see Supplementary Fig. S1) (Brenner, Tuvikene, Parker, Matsukawa, & Nishinari, 2014; Geonzon et al., 2019b). The stock solution of KCl was prepared by dissolving the powder in deionized water (Wako Pure Chemicals Ind., Ltd.).

2.2 Sample preparation

The samples for bulk rheology and microrheology experiments were prepared by using a simplified procedure described in the following references (Geonzon et al., 2019b; Geonzon, Zhuang, Santoya, Bacabac, Xie, & Matsukawa, 2020). The IC solutions, KCl solutions, deionized water (DI), and silica particles were mixed to obtain the desired concentration of carrageenan with 10 mM KCl, and ~0.001% w/w probe particles (for microrheology). The probe particles were non-functionalized silica with a net negative charge (diameter $2a$=1.0 μm, Nippon Shokubai, Japan) and suspended in DI (Elix Advantage 5, Millipore, Tokyo, Japan) (Kobayashi, Skarba, Galleto, Cakara, & Borkovec, 2005). The solution was then heated to 90 °C for 30 min with constant stirring. The hot

sample solutions were placed in a microscope chamber with double-sided tape as a spacer and sealed with vacuum sealant. Afterward, the sample was quenched to 5 °C to equilibrate and stored for 1-1.5 hours before measurement at 20 °C. Different carrageenan concentrations were studied from 0.5 wt. %-2.0 wt.%.

2.3 Bulk rheology

Bulk dynamic viscoelastic properties were measured using an OHNR1 rheometer (Model No.: OHNR1, OHNATECH, Japan) equipped with a concentric cylinder tool, having a gap of 1.65 mm. The temperature of the sample was regulated by using a temperature-controlled water bath. Hot sample solutions were loaded at ~70 °C. Prior to performing the measurements at 20 °C, the sample was quenched to ~15 °C to accelerate the gelation process and kept for 40-50 min at such temperature to fully equilibrate. A frequency sweep from 0.6 to 125 rad/s was performed at a constant strain amplitude of γ=0.01 to evaluate the frequency-dependent viscoelastic properties of the sample.

2.4 Passive microrheology

The microheological characterization protocols are schematically shown in Fig. 1. Passive microrheology was performed using a single-laser optical tweezer (wavelength λ=976 nm, OTKB/M, Thorlabs) as described in (Geonzon et al., 2021, 2022). The trapping laser was focused using a 100× oil immersion objective with a high numerical aperture (NA 1.25, WD 0.23 mm, Nikon) and then collected by an air condenser (10×, NA 0.25, WD 7 mm, Nikon). The fluctuation of the trapped particle was detected using a quadrant position detector (QPD) connected to the force measurement module (OTKBFM-CAL, Thorlabs).

The calibration factor of the voltage-to-position response function of the QPD was circa 0.80 V/μm.

The *x*- and *y*- coordinates of the optically trapped particle were recorded at a rate of 2 kHz for 700-800 seconds using the force acquisition module (OTKB-Cal, Thorlabs). The trap stiffness was set as low as possible (i.e., k_p=2.05×10^{-6} N/m) to allow thermal fluctuations of the probe particle. The position data were obtained by reformatting the measurable ones into time-series data, which consisted of time and converted *x*- and *y*-displacement expressed in micrometers by using a calibration factor (Mathematica 12.1, Wolfram Research, Inc., Champaign, IL). The particle positions were then analyzed, and in the case of linear viscoelastic measurements, the materials' properties were determined by using the analytical method described in (Tassieri, Evans, Warren, Bailey, & Cooper, 2012). Also, there is no significant changes in the thermal fluctuation of the trapped particle within the observation period implying that possible heating at the laser focus has a negligible effect in our study (Peterman, Gittes & Schmidt, 2003). For each sample, measurements were performed for at least five different particles.

In general, the thermal fluctuation of an optically trapped particle is affected by the response of the surrounding media and the trapping force (Mizuno et al., 2008; Tassieri, 2016). The thermal fluctuation of the probe particle can be analyzed by using the normalized position autocorrelation function, *NPAF*(τ), as described in (Tassieri, 2016; Tassieri et al., 2015):

$$NPAF(\tau) \equiv \frac{\langle \vec{x}(t)\vec{x}(t+\tau)\rangle_t}{\langle x^2\rangle_t} \quad (1)$$

where τ is the lag-time, $\vec{x}(t)$ is the particle position at time *t*, and $\langle x^2\rangle$ is the variance of the

particle trajectory. For sufficiently long measurements of the particle's thermal fluctuation suspended into a Newtonian fluid with viscosity η, the *NPAF*(τ) can be described by a single exponential decay function (Del Giudice et al., 2017; Tassieri, 2016)

$$NPAF(\tau) = e^{-\lambda\tau} \quad (2)$$

where $\lambda = k_p/\gamma$, k_p is the trap stiffness, and $\gamma = 6\pi a\eta$ is the friction coefficient (Tassieri, 2016; Tassieri et al., 2015).

In order to measure the linear viscoelastic properties of IC samples, we have employed the analytical method developed by (Tassieri et al., 2012), which relates the materials' shear complex modulus ($G^*(\omega)$) to the Fourier transform of the above-mentioned time-averaged fluctuation (Mason, Gang, Weitz, 1996; Pommella et al., 2013; Tassieri et al., 2010, 2015):

$$G^*(\omega) = G'(\omega) + iG''(\omega) = \frac{\hat{A}(\omega)}{\hat{\Pi}(\omega)} \quad (3)$$

Where $\hat{A}(\omega)$ and $\hat{\Pi}(\omega)$ are the Fourier transforms of $NPAF(\tau)$ and $NMSD(\tau)$, respectively.

2.5 Entraining flow measurement

The local structure of the gels was probed by imposing a large displacement, x_{disp}, of the particle embedded in the gel network (Fig. 1c), by following the procedure in reference (Chapman & Robertson-Anderson, 2014; Khan, Regan, & Robertson, 2019; Robertson-Anderson, 2018). The position of the optical trap was kept fixed in space while the sample was moved at different speeds, υ, using a 3-dimension translational stage (NanoMax 300, Thorlabs), which was controlled by custom software (LabVIEW). The applied stage movement, x_{stage}, and particle displacement relative to the optical trap centre, x_{disp}, were acquired at 10 Hz for 15 s as schematically shown in (Fig. 1). The x_{disp} was used to calculate the force exerted on the gel network, $F = k_A x_{disp}$; where the trap stiffness was set to a higher

value (k_A=2.25×10^{-5} N/m) than the one used for passive microrheology measurements. Before each measurement, a particle was trapped and allowed to equilibrate for 10-20 seconds. At least five different particles were measured for each speed at different regions throughout the sample. Repeats of each particle were not performed as the application of a large formation could have destroyed the gel network. The applied stage movement, x_{stage}, and the measured force, F, were converted to strain and stress by using the following relationships, $\gamma = x_{stage}/2a$ and $\sigma = F/\pi a^2$ (Robertson-Anderson, 2018). The applied strain rates were calculated by using the following relationship $\dot{\gamma} = 3v/\sqrt{2}a$. The details of these parameters are described in the Results and Discussion section. The experiments were all performed in a temperature-controlled room set at 20 °C.

3. Results and Discussion

3.1 Linear viscoelastic measurements

The thermal fluctuation of 1.0 μm diameter optically trapped particles embedded in the IC samples were used to determine the local rheological properties of the samples. In Fig. 2 (top) are reported the $NPAF(\tau)$ of the optically trapped particles embedded into five different samples. Whereas, in Fig. 2 (bottom) are reported the corresponding normalized mean square displacement curves, $NMSD(\tau)$; which are simply related to the $NPAF(\tau)$: $NMSD(\tau) = 1 - NPAF(\tau)$ (Preece et al., 2011). Notably, in the case of water, a good agreement between experiments and theoretical prediction (i.e., Eq. 2) is reported. Moreover, it is interestingly to notice that, at short time scales, the $NMSD(\tau)$ of the suspended particle in water shows a similar behaviour as for a freely diffusing particle, with a linear increase as function of the lag-time. At long lag-times, the $NMSD(\tau)$ approaches a plateau due to the

presence of trapping potential (Tassieri et al., 2010). Interestingly, in the case of particles embedded in IC samples, the $NPAF(\tau)$ does not follow a single relaxation mode (i.e., Eq. 2), which is highlighted by the lower value of the slope (i.e., <1) of the $NMSD(\tau)$ curves at short time scales. The decrease in the slope of $NMSD(\tau)$ at early time scale with increasing IC concentration can be attributed to the significant sub-diffusive behaviour of the particles governed by the increase of the viscoelastic nature of the sample. This behaviour is indeed typical of a non-Newtonian fluid and here it is due to the viscoelastic response provided by either the IC helices and aggregates in the solvent or the formation of the network structure of IC gels.

In Fig. 3 are reported the elastic modulus, $G'(\omega)$, and viscous modulus, $G''(\omega)$, as a function of frequency. Moreover, in order to reduce the amount of noise in the graphs, the moduli shown in Fig. 3 have been obtained by transforming a smooth fitting function of the experimental data shown in Fig. 2 (Tassieri et al., 2012). Nonetheless, the viscoelastic moduli obtained from a direct transformation of the experimental raw data were plotted for comparison, for which a good agreement can be observed. The crossover frequency is shown in Table 1. Moreover, the moduli obtained from the analysis of a measurement performed in water are also shown as a reference for the effective calibration of the passive microrheology measurements.

In Fig. 3, we also report the bulk rheological properties as a means of comparison with standard rheological measurements. In the case of IC samples, an apparent difference between the bulk and microrheological data can be observed. It appears that microrheology measurements underestimate the moduli by a factor of three to four times the bulk rheology

measurements. This kind of discrepancies have been observed also in other systems and has been attributed to either the differences between the length scales of the techniques or to the electrostatic interactions between the probe and polymer (Caggioni, Spicer, Blair, Linderberg, & Weitz, 2007; Cardinaux, Cipelletti, Scheffold, & Schurtenberger, 2002; Piechocka, Bacabac, Potters, Mackintosh, & Koenderink, 2010). An additional justification could be given by assuming the formation of a depletion layer surrounding the probe particles, given that both the probe particle and ι-carrageenan are negatively charged. This would result in a slight increase in the thermal fluctuation of the probe particle (Caggioni et al., 2007). Nonetheless, both techniques generally captured the behaviour of the frequency-dependent viscoelastic response of IC gels, with a good agreement between the two techniques in detecting the crossover frequency of the viscoelastic moduli of IC gels.

Moreover, from Fig. 3, the microrheological data obtained using optical tweezers show a wider viscoelastic spectrum than that bulk rheology could probe (Mizuno et al., 2008; Nishi, Kilfoil, Schmidt, & Mackintosh, 2018; Vyas et al., 2016; Yao et al., 2009). In particular, from Fig. 3, it is interesting to notice the change in behaviour of the viscoelastic moduli from IC at 1.5 wt.%, for which they show a viscous-dominated response, to the IC at 2.0 wt.% sample, for which they show a more elastic-dominated response. This is also corroborated by the time sweep measurements performed at 20 °C, as reported in Fig. S2 of the Supplementary. Nonetheless, a previous study shows that the onset of gelation for IC is expected at temperatures above 20 °C (Du et al., 2016). Therefore, we would expect the formation of helical aggregates of IC in our samples. However, the viscoelastic moduli of 2.0 wt.% IC are relatively low in magnitude, with a significant viscous component (i.e.,

285 $G''(\omega) > G'(\omega)/10$). Hence based on the consideration on the mechanical spectra of weak
286 gels wherein the moduli are slightly frequency dependent with $G''(\omega) > G'(\omega)/10$, it
287 implies that the IC gels considered in this study behave as weak-gels at this temperature
288 (Chronakis, Picullel, & Borgström, 1996; Ikeda & Nishinari, 2001).

289 In Fig. 4, we report the complex viscosity, $|\eta^*(\omega)| = |G^*(\omega)|/\omega$, as a function of
290 angular frequency at 20 °C obtained by reorganizing the data shown in Fig. 3. In the same
291 figure, the viscosity of water is also plotted as a means of comparison. Interestingly, at low
292 frequencies, all the IC samples show a frequency-independent behavior, with the onset of
293 the Newtonian plateau that shifts towards lower frequencies with increasing carrageenan
294 concentration. The plateau value of the complex viscosity provides a measure of the zero-
295 shear viscosity, η_0, which increases with polymer concentration due to the increase in the
296 number of entanglements within the network. At high frequencies, the drop of the $\eta^*(\omega)$ has
297 also been reported and attributed to the non-Newtonian behaviour of the IC, i.e., shear
298 thinning behaviour (Liu et al., 2015).

299 **3.2 Local strain-induced response**

300 In Fig. 5, we report the force exerted on the trapped particle during the stage movement
301 at different speeds. In order to interpret these measurements, we can recall the force response
302 for two extreme material properties, i.e., purely elastic solid and purely viscous fluid
303 (Chapman & Robertson-Anderson, 2014; Ricketts et al., 2019; Robertson-Anderson, 2018).
304 In particular, it is expected that, for a purely elastic material, the force would increase
305 linearly with applied stage movement, with the slope value providing a measure of the
306 network elastic properties. On the other hand, for a purely viscous solution, the force

307 response is expected to reach a plateau almost instantaneously, with force magnitude
308 proportional to the strain rate (Ricketts et al., 2019).

309 In Fig. 5, the force responses for both 1.5 wt.% and 2.0 wt.% IC samples show an
310 intermediate behaviour between the extreme cases, in agreement with the viscoelastic nature
311 of the materials. In particular, in the case of 1.5 wt.% IC, the force increases rapidly at short
312 times (i.e., high frequencies), and then at relatively long times (i.e., low frequencies), it
313 approaches a plateau. Therefore, the initial increase is a measure of the local elastic
314 properties of the material, whereas, at long times (i.e., by imposing large deformation), the
315 material yields and behaves like a viscous fluid. It is interesting to notice that the yielding
316 force increases with the increase of stage velocity or equivalently the strain rate. The
317 magnitude of the yielding force, F_y, provides a measure of the elasticity of the material. This
318 is confirmed by the response of the 2.0 wt.% IC, which shows a different force response
319 than the 1.5 wt.% IC. Although the 2.0 wt.% IC is considered to be a weak gel, but the fact
320 that G' is larger than G'' implies the presence of the highly entangled network. Hence, the
321 sample shows larger resistive forces and does not exhibit any yielding within the explored
322 stage velocities, thus reflecting the formation of a highly entangled network of IC gels. This
323 is further corroborated by the speed at which the force response curve of 2.0 wt.% IC returns
324 to zero when the stage stops, as the elastic component of the material would complement
325 the restoring force by the optical trap.

326 In order to better understand the materials' behavior in terms of the force response curve,
327 the measured force, F, and applied stage displacement, x_{stage}, were converted into stress, σ,
328 and strain, γ, by means of the following two relationships: $\sigma = F/\pi a^2$ and $\gamma = x_{stage}/2a$

329 (Chapman & Robertson-Anderson, 2014; Robertson-Anderson, 2018), and reported in Fig.
330 6. For all samples, the initial increase in the σ with increasing γ can be attributed to the
331 elastic character of the material at high frequencies, which is mostly related to the stiffness
332 (i.e. $G'(\omega)$) of the network (Fig. 7a). For a 1.5 wt.% IC, yielding was observed for all strain
333 rates, demonstrating a more viscous response. Also, the yield strain roughly increases with
334 the increase in strain rate. The yielding behavior of 1.5 wt.% ICgf implies permanent
335 deformation with the applied large strains. In the linear rheological measurements (Fig. 3),
336 the 1.5 wt.% sample showed viscoelastic fluid properties suggesting the formation of a non-
337 permanent network of IC helices at these conditions of polymer concentration and
338 temperature. Furthermore, the same yielding phenomena were observed in the case of the
339 concentrated DNA and F-actin network studied using the same technique, attributed to the
340 release of entanglements in the network (Chapman & Robertson-Anderson, 2014; Falzone
341 et al., 2015). Therefore, the yielding can be attributable to the irreversible microstructure
342 rearrangement, possibly due to the disentanglement of IC helices, which are responsible for
343 the viscoelastic properties of IC.

344 On the contrary, the 2.0 wt.% IC exhibited the gel-like behavior in agreement with the
345 linear rheological measurements (see Fig. 3), suggesting a highly entangled network of IC
346 helices. Moreover, a clear dependence on the strain rates was observed for 2.0 wt.% IC.
347 While a plateau region in the stress at intermediate strain was observed at lower strain rates
348 (below 0.16 μm/s), the stress continuously increased with strain at higher strain rates. The
349 plateau value of the stress at lower rates could be attributed to the possible rearrangement
350 of the IC aggregates to accommodate the applied deformation. After the plateau, an increase

in stress was also demonstrated with a further increase in strain. The plateau diminished with increasing the strain rate. This diminished strain could be explained as follows: as the strain rate increases, the time for the microstructure rearrangement is too short. Moreover, highly crosslinked microtubules demonstrated similar elastic responses. This was considered to originate from the degree of crosslinking in the microtubule network (Ricketts et al., 2019). Hence, it can be considered that the increase in the polymer concentration contributes to more entanglement that enhances the elastic properties and restrains possible rearrangement of the network with large deformation.

The rheological parameters were calculated from the σ and γ curves as a function of $\dot{\gamma}$, as shown in Fig. 7. Fig. 7a presents the initial slope of σ and γ, $(d\sigma/d\gamma)_{\gamma\to 0}$ as a function of $\dot{\gamma}$, calculated at the initial increase of σ. As mentioned earlier, the $d\sigma/d\gamma$ is comparable to the stiffness of the network or differential modulus, K (Robertson-Anderson, 2018). For a 2.0 wt.% IC, the $d\sigma/d\gamma$ is almost independent of $\dot{\gamma}$ showing a gel-like behavior. On the contrary, a clear dependence of $d\sigma/d\gamma$ on $\dot{\gamma}$ was seen for 1.5 wt.% IC. Furthermore, the $d\sigma/d\gamma$ showed a tendency to approach a constant value with increasing $\dot{\gamma}$. The same behaviour was also seen for F-actin gels using the same methodology (Falzone et al., 2015). We consider that the dependence of $d\sigma/d\gamma$ on $\dot{\gamma}$ can be attributed to the network properties and rearrangement of IC helices with the applied local deformation. By giving enough time at low strain rates, the possible network rearrangement contributes to stress dissipation. Moreover, with increasing strain rates, the time required for network rearrangement may not be enough, contributing to the elastic response of the material, which originates from the entangled network. Fig. 7b presents the average yield stress, σ_y against $\dot{\gamma}$. From the σ_y, the apparent

viscosity, η, was calculated following the Stokes relationship based on the magnitude of the yielding force, F_y, as shown in the following equation: $\eta = F_y/6\pi a v$, and considering $\sigma_y = F_y/\pi a^2$ (Robertson-Anderson, 2018). The apparent viscosity, η against $\dot{\gamma}$ are shown in Fig. 7c. For all concentrations, the η decreases with strain rate indicating a shear thinning behaviour of IC in agreement with the macroscopic measurements (Chronakis et al., 2000). The shear thinning exponents is higher than -1.0, which is an apparent limit for well-entangled polymer solutions (Teixeira et al., 2007). Moreover, the $\eta^*(\omega)$ obtained using passive microrheology (Fig. 4) exhibited shear thinning behaviour at high frequencies with exponent ≈-1.0 and a plateau at low frequencies. Despite the difference in the methodologies, the viscosities obtained from both passive and large deformation microrheology are within the same orders of magnitude. Furthermore, it has been found that dilute polymer solutions demonstrate shear thinning exponent even up to circa -0.5. This suggests that our samples can be considered within the entangled regime, and the material properties comes from the entanglement of rigid IC helices (Ikeda & Nishinari, 2001; Morris et al., 1999).

3.3 Proposed structure developed from different investigations

Based on the above discussion and previous results from different investigations, the network of IC gels is schematically drawn in Fig. 8. Previous study on the gelation mechanism and network structure of IC gels at submicroscopic viewpoints suggest the formation of clusters of IC aggregates (Geonzon *et al*., 2019b). This submicroscopic investigation supports the macroscopic measurements using bulk rheology of IC gels (Du *et al.*, 2016; Hu *et al.*, 2016; Takemasa *et al.*, 2001). The microrheological results presented in this study, both in linear and nonlinear regimes, corroborate the macroscopic and

submicroscopic results. Moreover, the wide spectral content captured by using passive microrheology suggests that the viscoelastic properties of IC originates from the entanglement of rigid IC helices. This is further confirmed by the large deformation measurements, which infer that the yielding at low IC concentration comes from the rearrangement of clusters and disentanglement of rigid IC helices. Increasing the IC concentration and entanglement density suppresses the yielding and produces a gel-like behaviour, which may suggest that the systems may be composed of non-percolating clusters of IC chain aggregates. These aggregated IC chains contribute to IC gels' rheological properties, even without forming permanent networks and allow particle diffusion, as seen in the diffusion measurements. Thus, we infer the schematic illustration shown in Fig. 8 as heterogenous clusters of IC helices developed from different perspectives.

4. Conclusion

We have performed optical tweezers-based microrheology to gain new insights into the hierarchical network structure of IC gels. Two microrheological techniques were employed to probe the network structure: passive microrheology and local large deformation measurements. Comparison between bulk and passive microrheology showed slight differences attributed to the difference in detecting length scale, but captured the behaviour of the materials' frequency-dependent viscoelastic properties. By applying large deformation to the local network structure of IC gels, we gained further information on the hierarchical structure of IC gels. In particular, we have found a concentration-dependent nonlinear responses of the IC gels at the mesoscopic scales. At concentrations <2.0 wt.%,

IC samples yield with the application of large deformation because of the rearrangement of clusters and disentanglement of the IC helices. In contrast, at 2.0 wt.%, the high entanglement density suppresses the rearrangement of clusters, and the sample exhibits a gel-like behaviour. To the best of our knowledge, this is the first time to explore the mesoscopic properties of the IC gels.

Author Contributions

Lester Geonzon: Conceptualization, Methodology, Software, Visualization, Formal Analysis, Investigation, Writing-Original Draft, Writing - Review & Editing. **Motoyoshi Kobayashi**: Supervision; Conceptualization; Methodology; Formal analysis; Validation; Visualization; Writing-original draft; Writing-review & editing; Resources; Funding acquisition; Project administration. **Manlio Tassieri:** Formal analysis; Software; Writing-review & editing. **Rommel Bacabac:** Formal Analysis; Writing - Review & Editing. **Yasuhisa Adachi**: Funding acquisition; Project administration. **Shingo Matsukawa:** Formal Analysis; Resources; Writing - Review & Editing.

Conflicts of interest

There are no conflicts of interest to declare.

Acknowledgment

The authors are grateful for the financial support of JSPS KAKENHI Grant Number 20F20388, 22H00387, and 19H03070. RG Bacabac was funded by DOST through the S4CP-CRADLE project No. 8448, monitored by DOST-PCIEERD, and received logistic support from the USC Research Office and Department of Physics.

437

438 **References**

439 Amici, E., Clark, A. H., Normand, V., & Johnson, N. B. (2001). Interpenetrating network
440 formation in agarose-sodium gellan gel composites. *Carbohydrate Polymers*, *46*(4),
441 383–391. https://doi.org/10.1016/S0144-8617(00)00342-8

442 Ashkin, A., Dziedzic, D., Bjorkholm, J. E., & Chu, S. (1986). Observation of a single-beam
443 gradient force optical trap for dielectric particles. *Optics Letters*, *11*(5), 288–290.

444 Azevedo, G., Torres, M. D., Sousa-Pinto, I., & Hilliou, L. (2015). Effect of pre-extraction
445 alkali treatment on the chemical structure and gelling properties of extracted hybrid
446 carrageenan from Chondrus crispus and Ahnfeltiopsis devoniensis. *Food*
447 *Hydrocolloids*, *50*, 150–158. https://doi.org/10.1016/j.foodhyd.2015.03.029

448 Bai, R. G., & Tuvikene, R. (2021). Potential antiviral properties of industrially important
449 marine algal polysaccharides and their significance in fighting a future viral pandemic.
450 *Viruses*, *13*(9). https://doi.org/10.3390/v13091817

451 Barabanova, A. O., Shashkov, A. S., Glazunov, V. P., Isakov, V. V., Nebylovskaya, T. B.,
452 Helbert, W., Solov'eva, T. F., & Yermak, I. M. (2008). Structure and properties of
453 carrageenan-like polysaccharide from the red alga Tichocarpus crinitus (Gmel.) Rupr.
454 (Rhodophyta, Tichocarpaceae). *Journal of Applied Phycology*, *20*(6), 1013–1020.
455 https://doi.org/10.1007/s10811-007-9295-z

456 Berg-Sørensen, K., & Flyvbjerg, H. (2004). Power spectrum analysis for optical tweezers.
457 *Review of Scientific Instruments*, *75*(3), 594–612. https://doi.org/10.1063/1.1645654

458 Brenner, T., Tuvikene, R., Parker, A., Matsukawa, S., & Nishinari, K. (2014). Rheology and

structure of mixed kappa-carrageenan/iota-carrageenan gels. *Food Hydrocolloids*, *39*, 272–279. https://doi.org/10.1016/j.foodhyd.2014.01.024

Bui, V. T. N. T., Nguyen, B. T., Nicolai, T., & Renou, F. (2019). Mobility of carrageenan chains in iota- and kappa carrageenan gels. *Colloids and Surfaces A: Physicochemical and Engineering Aspects*, *562*(October 2018), 113–118. https://doi.org/10.1016/j.colsurfa.2018.11.017

Caggioni, M., Spicer, P. T., Blair, D. L., Lindberg, S. E., & Weitz, D. A. (2007). Rheology and microrheology of a microstructured fluid: The gellan gum case. *Journal of Rheology*, *51*(5), 851–865. https://doi.org/10.1122/1.2751385

Cao, W., Jin, J., Wu, G., Bravenboer, N., Helder, M. N., Pathak, J. L., Zandieh-Doulabi, B., Hogervorst, J. M. A., Matsukawa, S., Geonzon, L. C., Bacabac, R. G., Schulten, E. A. J. M., & Klein-Nulend, J. (2021). K-carrageenan stimulates pre-osteoblast proliferation and osteogenic differentiation: A potential factor for the promotion of bone regeneration? *Molecules*, *26*(20). https://doi.org/10.3390/molecules26206131

Cardinaux, F., Cipelletti, L., Scheffold, F., & Schurtenberger, P. (2002). Microrheology of giant-micelle solutions. *Europhysics Letters*, *57*(5), 738–744. https://doi.org/10.1209/epl/i2002-00525-0

Chapman, C. D., & Robertson-Anderson, R. M. (2014). Nonlinear microrheology reveals entanglement-driven molecular-level viscoelasticity of concentrated DNA. *Physical Review Letters*, *113*(9), 1–5. https://doi.org/10.1103/PhysRevLett.113.098303

Chronakis, I. S., Doublier, J. L., & Piculell, L. (2000). Viscoelastic properties for kappa- and iota-carrageenan in aqueous NaI from the liquid-like to the solid-like behaviour.

International Journal of Biological Macromolecules, *28*(1), 1–14. https://doi.org/10.1016/S0141-8130(00)00141-0

Chronakis, I. S., Piculell, L., & Borgström, J. (1996). Rheology of kappa-carrageenan in mixtures of sodium and cesium iodide: Two types of gels. *Carbohydrate Polymers*, *31*(4), 215–225. https://doi.org/10.1016/S0144-8617(96)00117-8

Del Giudice, F., Tassieri, M., Oelschlaeger, C., & Shen, A. Q. (2017). When Microrheology, Bulk Rheology, and Microfluidics Meet: Broadband Rheology of Hydroxyethyl Cellulose Water Solutions. *Macromolecules*, *50*(7), 2951–2963. https://doi.org/10.1021/acs.macromol.6b02727

Du, L., Brenner, T., Xie, J., & Matsukawa, S. (2016). A study on phase separation behavior in kappa/iota carrageenan mixtures by micro DSC, rheological measurements and simulating water and cations migration between phases. *Food Hydrocolloids*, *55*(July 2018), 81–88. https://doi.org/10.1016/j.foodhyd.2015.11.004

Falzone, T. T., Blair, S., & Robertson-Anderson, R. M. (2015). Entangled F-actin displays a unique crossover to microscale nonlinearity dominated by entanglement segment dynamics. *Soft Matter*, *11*(22), 4418–4423. https://doi.org/10.1039/c5sm00155b

Geonzon, L. C., Bacabac, R. G., & Matsukawa, S. (2019a). Microscopic Characterization of Phase Separation in Mixed Carrageenan Gels Using Particle Tracking. *Journal of The Electrochemical Society*, *166*(9), B3228–B3234. https://doi.org/10.1149/2.0351909jes

Geonzon, L. C., Bacabac, R. G., & Matsukawa, S. (2019b). Network structure and gelation mechanism of kappa and iota carrageenan elucidated by multiple particle tracking.

Food Hydrocolloids, *92*, 173–180. https://doi.org/10.1016/j.foodhyd.2019.01.062

Geonzon, L. C., Descallar, F. B. A., Du, L., Bacabac, R. G., & Matsukawa, S. (2020). Gelation mechanism and network structure in gels of carrageenans and their mixtures viewed at different length scales – A review. *Food Hydrocolloids*, *108*, 106039. https://doi.org/10.1016/j.foodhyd.2020.106039

Geonzon, L. C., Kobayashi, M., & Adachi, Y. (2021). Effect of shear flow on the hydrodynamic drag force of a spherical particle near a wall evaluated using optical tweezers and microfluidics. *Soft Matter*, *17*(34), 7914–7920. https://doi.org/10.1039/d1sm00876e

Geonzon, L. C., Kobayashi, M., Sugimoto, T., & Adachi, Y. (2022). Study on the Kinetics of Adsorption of Poly(ethylene oxide) Onto A Silica Particle Using Optical Tweezers and Microfluidics. *Colloids and Surfaces A: Physicochemical and Engineering Aspects*, *642*(February), 128691. https://doi.org/10.1016/j.colsurfa.2022.128691

Geonzon, L. C., Zhuang, X., Santoya, A. M., Bacabac, R. G., Xie, J., & Matsukawa, S. (2020). Gelation mechanism and network structure of mixed kappa carrageenan/lambda carrageenan gels studied by macroscopic and microscopic observation methods. *Food Hydrocolloids*, *105*, 105759. https://doi.org/10.1016/j.foodhyd.2020.105759

Gomez-Solano, J. R., & Bechinger, C. (2014). Probing linear and nonlinear microrheology of viscoelastic fluids. *Epl*, *108*(5). https://doi.org/10.1209/0295-5075/108/54008

Gomez-Solano, Juan Ruben, & Bechinger, C. (2015). Transient dynamics of a colloidal particle driven through a viscoelastic fluid. *New Journal of Physics*, *17*(10).

https://doi.org/10.1088/1367-2630/17/10/103032

Hori, K., Penaloza, D. P., Shundo, A., & Tanaka, K. (2012). Time-dependent heterogeneity in viscoelastic properties of worm-like micelle solutions. *Soft Matter*, *8*(28), 7361–7364. https://doi.org/10.1039/c2sm25549a

Hu, B., Du, L., & Matsukawa, S. (2016). NMR study on the network structure of a mixed gel of kappa and iota carrageenans. *Carbohydrate Polymers*, *150*, 57–64. https://doi.org/10.1016/j.carbpol.2016.04.112

Ikeda, S., & Nishinari, K. (2001). *" Weak Gel " -Type Rheological Properties of Aqueous Dispersions of Nonaggregated K -Carrageenan Helices*. 4436–4441.

Khan, M., Regan, K., & Robertson-Anderson, R. M. (2019). Optical Tweezers Microrheology Maps the Dynamics of Strain-Induced Local Inhomogeneities in Entangled Polymers. *Physical Review Letters*, *123*(3), 38001. https://doi.org/10.1103/PhysRevLett.123.038001

Kobayashi, M., Skarba, M., Galletto, P., Cakara, D., & Borkovec, M. (2005). Effects of heat treatment on the aggregation and charging of Stöber-type silica. *Journal of Colloid and Interface Science*, *292*(1), 139–147. https://doi.org/10.1016/j.jcis.2005.05.093

Liu, S., Chan, W. L., & Li, L. (2015). Rheological Properties and Scaling Laws of κ-Carrageenan in Aqueous Solution. *Macromolecules*, *48*(20), 7649–7657. https://doi.org/10.1021/acs.macromol.5b01922

Maki, Y., & Annaka, M. (2020). Gelation of fish gelatin studied by multi-particle tracking method. *Food Hydrocolloids*, *101*(November 2019), 105525. https://doi.org/10.1016/j.foodhyd.2019.105525

547 Mason, T. G. (2000). Estimating the viscoelastic moduli of complex fluids using the
548 generalized Stokes-Einstein equation. *Rheologica Acta*, *39*(4), 371–378.
549 https://doi.org/10.1007/s003970000094
550 Mason, T. G., Gang, H., & Weitz, D. A. (1996). Rheology of complex fluids measured by
551 dynamic light scattering. *Journal of Molecular Structure*, *383*(1–3), 81–90.
552 https://doi.org/10.1016/S0022-2860(96)09272-1
553 Mizuno, D., Head, D. A., MacKintosh, F. C., & Schmidt, C. F. (2008). Active and passive
554 microrheology in equilibrium and nonequilibrium systems. *Macromolecules*, *41*(19),
555 7194–7202. https://doi.org/10.1021/ma801218z
556 Morris, V. J., Kirby, A. R., & Gunning, A. P. (1999). A fibrous model for gellan gels from
557 atomic force microscopy studies. *Progress in Colloid and Polymer Science*, *114*, 102–
558 108. https://doi.org/10.1007/3-540-48349-7_15
559 Mundo, J. L. M., Zhou, H., Tan, Y., Liu, J., & McClements, D. J. (2021). Enhancing
560 emulsion functionality using multilayer technology: Coating lipid droplets with
561 saponin-polypeptide-polysaccharide layers by electrostatic deposition. *Food Research*
562 *International*, *140*(April), 109864. https://doi.org/10.1016/j.foodres.2020.109864
563 Necas, J., & Bartosikova, L. (2013). Carrageenan: A review. *Veterinarni Medicina*, *58*(4),
564 187–205. https://doi.org/10.17221/6758-VETMED
565 Nishi, K., Kilfoil, M. L., Schmidt, C. F., & Mackintosh, F. C. (2018). A symmetrical method
566 to obtain shear moduli from microrheology. *Soft Matter*, *14*(19), 3716–3723.
567 https://doi.org/10.1039/c7sm02499a
568 Peterman, E. J. G., Gittes, F., & Schmidt, C. F. (2003). Laser-induced heating in optical traps.

569 *Biophysical Journal*, *84*(2 I), 1308–1316. https://doi.org/10.1016/S0006-
570 3495(03)74946-7
571 Piechocka, I. K., Bacabac, R. G., Potters, M., Mackintosh, F. C., & Koenderink, G. H. (2010).
572 Structural hierarchy governs fibrin gel mechanics. *Biophysical Journal*, *98*(10), 2281–
573 2289. https://doi.org/10.1016/j.bpj.2010.01.040
574 Pommella, A., Preziosi, V., Caserta, S., Cooper, J. M., Guido, S., & Tassieri, M. (2013).
575 Using optical tweezers for the characterization of polyelectrolyte solutions with very
576 low viscoelasticity. *Langmuir*, *29*(29), 9224–9230. https://doi.org/10.1021/la4015948
577 Preece, D., Warren, R., Evans, R. M. L., Gibson, G. M., Padgett, M. J., Cooper, J. M., &
578 Tassieri, M. (2011). Optical tweezers: Wideband microrheology. *Journal of Optics*,
579 *13*(4). https://doi.org/10.1088/2040-8978/13/4/044022
580 Rees, D. A., Steele, I. W., & Williamson, F. B. (1969). Conformational analysis of
581 polysaccharides. III. The relation between stereochemistry and properties of some
582 natural polysaccharide sulfates (1). *Journal of Polymer Science Part C: Polymer*
583 *Symposia*, *28*(1), 261–276. https://doi.org/10.1002/polc.5070280121
584 Ricketts, S. N., Francis, M. L., Farhadi, L., Rust, M. J., Das, M., Ross, J. L., & Robertson-
585 Anderson, R. M. (2019). Varying crosslinking motifs drive the mesoscale mechanics
586 of actin-microtubule composites. *Scientific Reports*, *9*(1), 1–12.
587 https://doi.org/10.1038/s41598-019-49236-4
588 Robal, M., Brenner, T., Matsukawa, S., Ogawa, H., Truus, K., Rudolph, B., & Tuvikene, R.
589 (2017). Monocationic salts of carrageenans: Preparation and physico-chemical
590 properties. *Food Hydrocolloids*, *63*, 656–667.

https://doi.org/10.1016/j.foodhyd.2016.09.032

Robertson-Anderson, R. M. (2018). Optical Tweezers Microrheology: From the Basics to Advanced Techniques and Applications. *ACS Macro Letters*, *7*(8), 968–975. https://doi.org/10.1021/acsmacrolett.8b00498

Rochas, C., Rinaudo, M., & Landry, S. (1989). Relation between the molecular structure and mechanical properties of carrageenan gels. *Carbohydrate Polymers*, *10*(2), 115–127. https://doi.org/10.1016/0144-8617(89)90061-1

Roesch, R., Cox, S., Compton, S., Happek, U., & Corredig, M. (2004). κ-Carrageenan and β-lactoglobulin interactions visualized by atomic force microscopy. *Food Hydrocolloids*, *18*(3), 429–439. https://doi.org/10.1016/j.foodhyd.2003.08.001

Shindel, M. M., & Furst, E. M. (2015). Frequency modulated microrheology. *Lab Chip*, *15*(11), 2460–2466. https://doi.org/10.1039/C5LC00351B

Simeone, M., Tassieri, M., Sibillo, V., & Guido, S. (2005). Effect of sol-gel transition on shear-induced drop deformation in aqueous mixtures of gellan and κ-carrageenan. *Journal of Colloid and Interface Science*, *281*(2), 488–494. https://doi.org/10.1016/j.jcis.2004.08.095

Svoboda, K., Schmidt, C. F., Schnapp, B. J., & Block, B. S. M. (1993). Direct observation of kinesin stepping by OT interferometry. *Nature*, *365*(October), 721–727.

Takemasa, M., Chiba, A., & Date, M. (2001). Gelation mechanism of κ- and ι-carrageenan investigated by correlation between the strain-optical coefficient and the dynamic shear modulus. *Macromolecules*, *34*(21), 7427–7434. https://doi.org/10.1021/ma0102924

Tassieri, M. (2016). *Microrheology with Optical Tweezers: Principles and Applications*. Pan

613 Stanford Publishing Pte. Ltd.
614 Tassieri, M., Del Giudice, F., Robertson, E. J., Jain, N., Fries, B., Wilson, R., Glidle, A.,
615 Greco, F., Netti, P. A., Maffettone, P. L., Bicanic, T., & Cooper, J. M. (2015).
616 Microrheology with optical tweezers: Measuring the relative viscosity of solutions “at
617 a glance.” *Scientific Reports*, *5*, 1–6. https://doi.org/10.1038/srep08831
618 Tassieri, M., Evans, R. M. L., Warren, R. L., Bailey, N. J., & Cooper, J. M. (2012).
619 Microrheology with optical tweezers: Data analysis. *New Journal of Physics*, *14*.
620 https://doi.org/10.1088/1367-2630/14/11/115032
621 Tassieri, M., Gibson, G. M., Evans, R. M. L., Yao, A. M., Warren, R., Padgett, M. J., &
622 Cooper, J. M. (2010). Measuring storage and loss moduli using optical tweezers:
623 Broadband microrheology. *Physical Review E - Statistical, Nonlinear, and Soft Matter*
624 *Physics*, *81*(2), 1–5. https://doi.org/10.1103/PhysRevE.81.026308
625 Teixeira, R. E., Dambal, A. K., Richter, D. H., Shaqfeh, E. S. G., & Chu, S. (2007). The
626 individualistic dynamics of entangled DNA in solution. *Macromolecules*, *40*(7), 2461–
627 2476. https://doi.org/10.1021/ma062932e
628 Thrimawithana, T. R., Young, S., Dunstan, D. E., & Alany, R. G. (2010). Texture and
629 rheological characterization of kappa and iota carrageenan in the presence of counter
630 ions. *Carbohydrate Polymers*, *82*(1), 69–77.
631 https://doi.org/10.1016/j.carbpol.2010.04.024
632 Usov, A. I. (1992). Sulfated polysaccharides of the red seaweeds. *Topics in Catalysis*, *6*(1),
633 9–23. https://doi.org/10.1016/S0268-005X(09)80055-6
634 Van Mameren, J., Modesti, M., Kanaar, R., Wyman, C., Wuite, G. J. L., & Peterman, E. J.

G. (2006). Dissecting elastic heterogeneity along DNA molecules coated partly with Rad51 using concurrent fluorescence microscopy and optical tweezers. *Biophysical Journal*, *91*(8), L78–L80. https://doi.org/10.1529/biophysj.106.089466

Vyas, B. M., Orpe, A. V., Kaushal, M., Joshi, Y. M., Joshi, Y. M., Cicuta, P., Donald, A. M., Squires, T. M., Mason, T. G., Puertas, A. M., Voigtmann, T., Schultz, K. M., Furst, E. M., Abdala, A. A., Amin, S., Zanten, J. H. van, Khan, S. A., Moschakis, T., Fielding, S. M., … Sasso, A. (2016). Passive microrheology in the effective time domain: analyzing time dependent colloidal dispersions. *Soft Matter*, *5*, 181–202. https://doi.org/10.1039/C6SM00829A

Waigh, T. A. (2016). Advances in the microrheology of complex fluids. *Reports on Progress in Physics*, *074601*, 1–101. https://doi.org/10.1088/0034-4885/79/7/074601

Yang, N., Lv, R., Jia, J., Nishinari, K., & Fang, Y. (2017). Application of Microrheology in Food Science. *Annual Review of Food Science and Technology*, *8*(January), 493–521. https://doi.org/10.1146/annurev-food-030216-025859

Yao, A., Tassieri, M., Padgett, M., & Cooper, J. (2009). Microrheology with optical tweezers. *Lab on a Chip*, *9*(17), 2568–2575. https://doi.org/10.1039/b907992k

Zhao, Q., & Matsukawa, S. (2012). Estimation of the hydrodynamic screening length in -carrageenan solutions using NMR diffusion measurements. *Polymer Journal*, *44*(8), 901–906. https://doi.org/10.1038/pj.2012.107

Table 1. The crossover frequency of G′ and G″ obtained using both techniques

	0.5 wt.%	**1.0 wt.%**	**1.5 wt.%**		**2.0 wt.%**	
			Bulk	**OT**	**Bulk**	**OT**
ω /rad/s	875.3	257.5	125.7	71.6	2.0	1.9

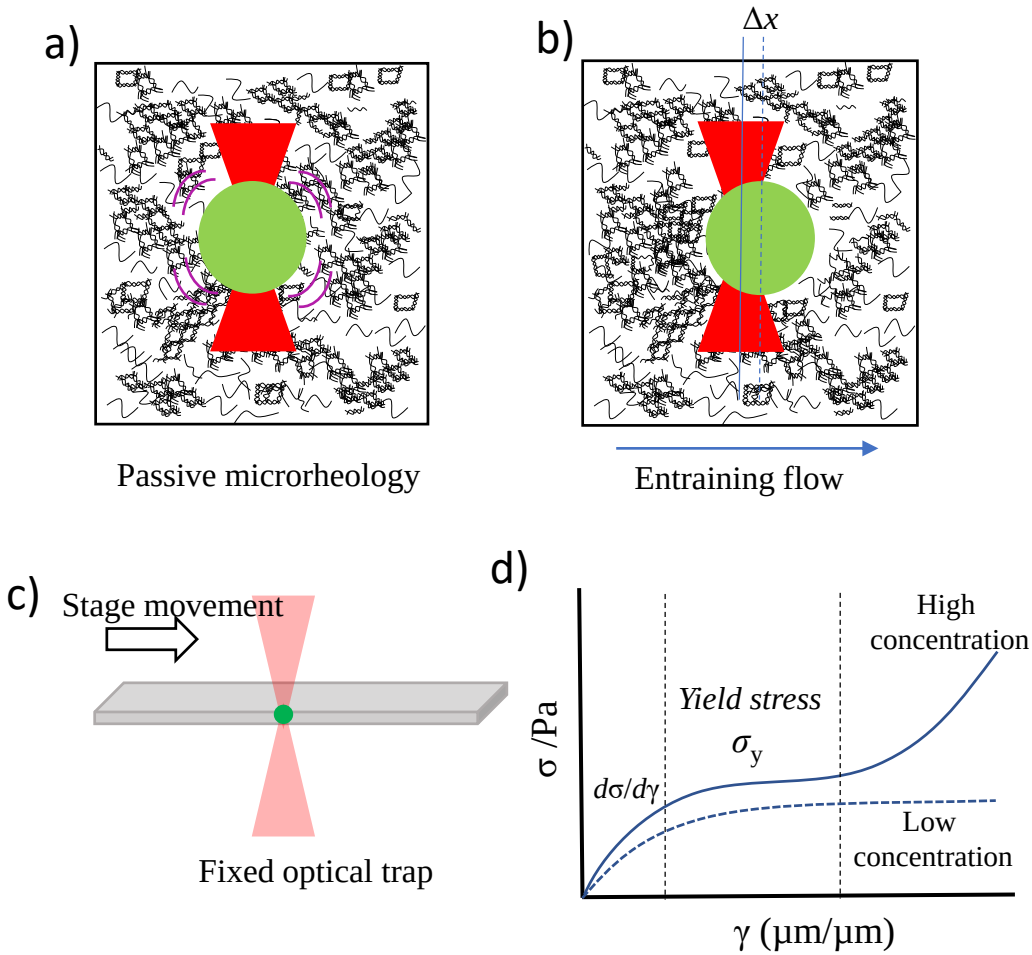

Fig. 1. Protocols for the microrheological characterization of the ι-carrageenan gels using optical tweezer. a) Passive microrheology and b) entraining flow for large deformation measurement. c) For the entraining flow, the sample stage is moved at different rates over a distance *x* and the force *F* the sample exerts on the trapped particle is measured d) Schematic illustration of the stress, σ, and strain, γ, curve. The green balls in Figs. 1 a-c represent the probe particle. Meanwhile, the black curves/lines in Figs. 1 a-b represent the IC polymers and the aggregates. The purple curves in Fig. 1a represents the fluctuation of the trapped particle for the passive microrheology measurements. Finally, the red trapezoids in Figs. 1 a-c represents the trapping laser that is highly focused after passing through the objective lens.

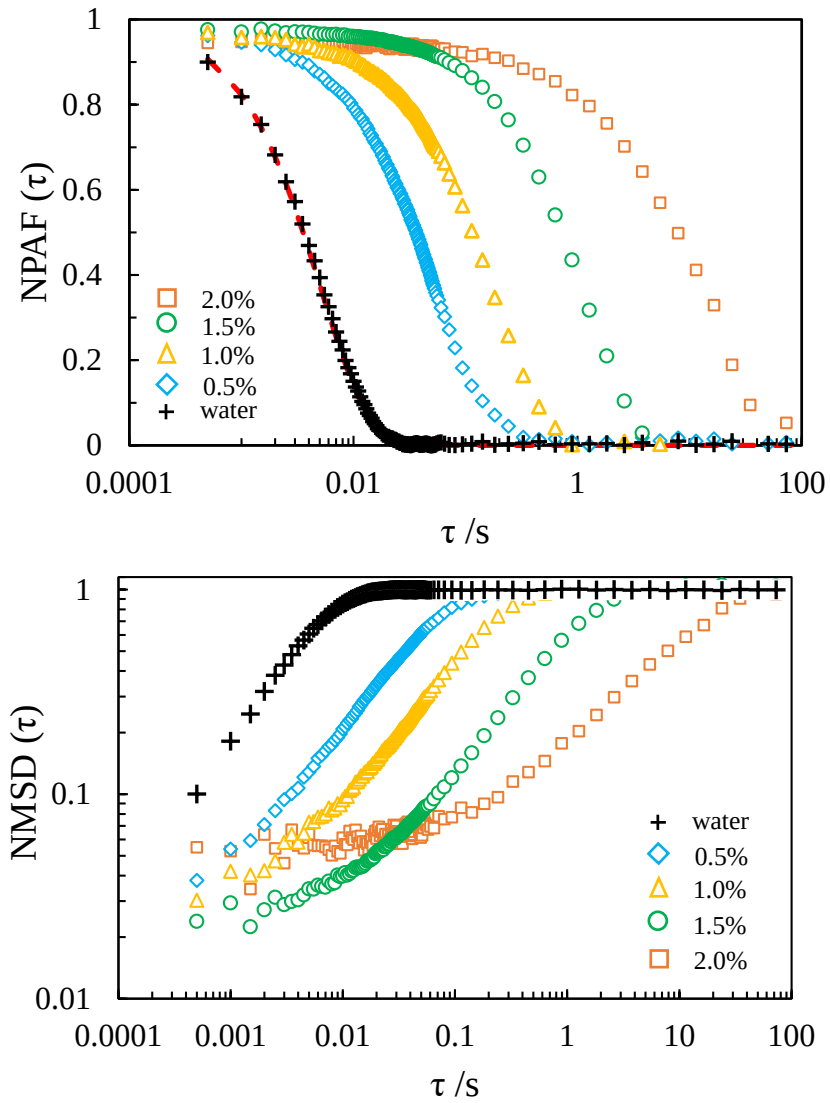

Fig. 2. (Top) Normalized position autocorrelation function, *NPAF*(τ), and (bottom) normalized mean square displacement, *NMSD*(τ), plots of an optically trapped particle ($2a$ = 1 μm) in IC gels measured at 2 kHz for a period of 700-800 s at laser current of 50 mA (k~2.05×10^{-6} N/m). Water data was only measured for 300 s.

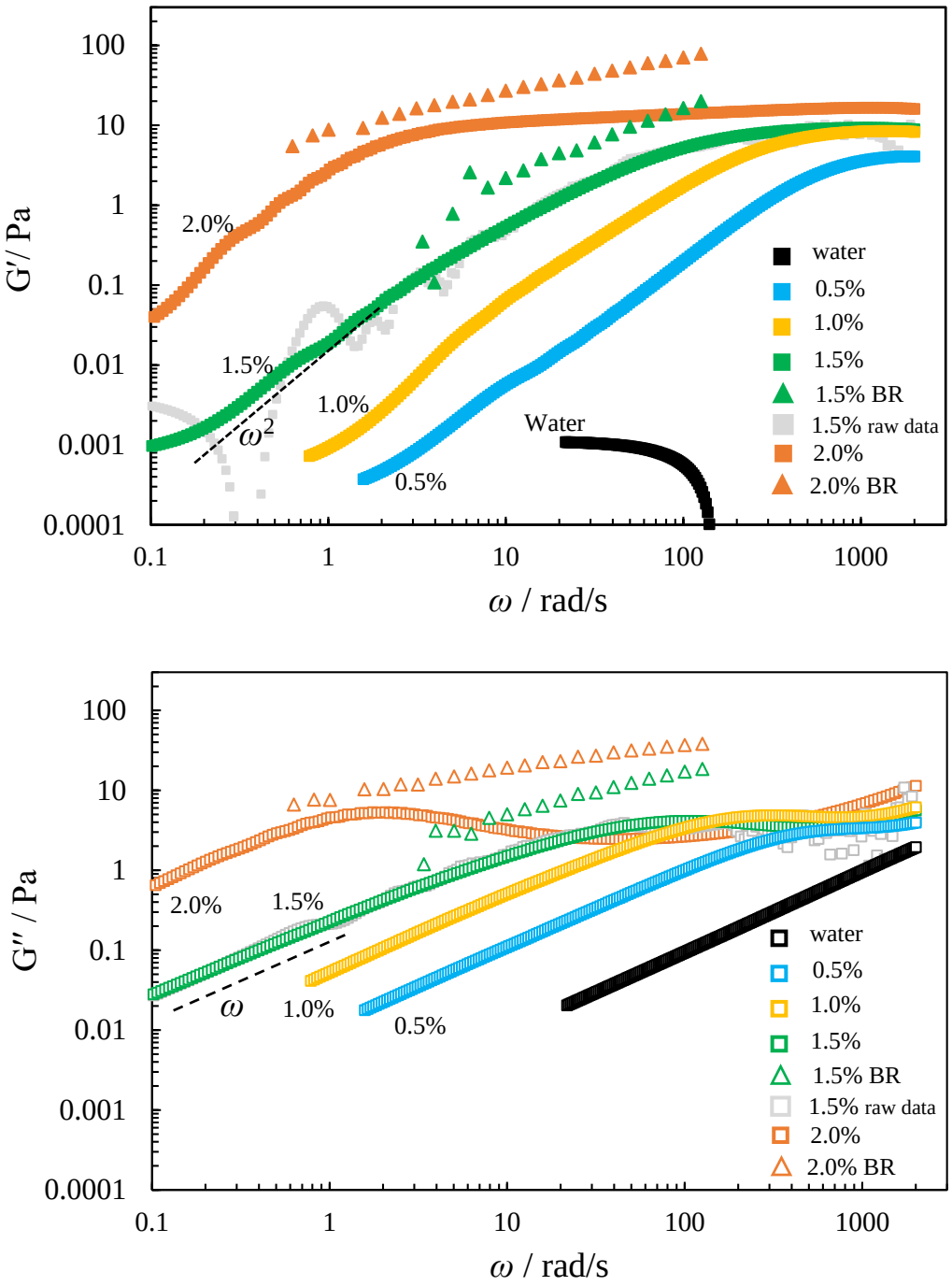

Fig. 3. Plots of viscoelastic moduli (top) *G′* (filled) and (bottom) G″ (open) as a function of frequency obtained using passive microrheology (square) and bulk rheology (BR) (triangle) measurement. The micorheology data using OT were obtained using the fitting function from the raw experimental data (i.e., 1.5% raw data).

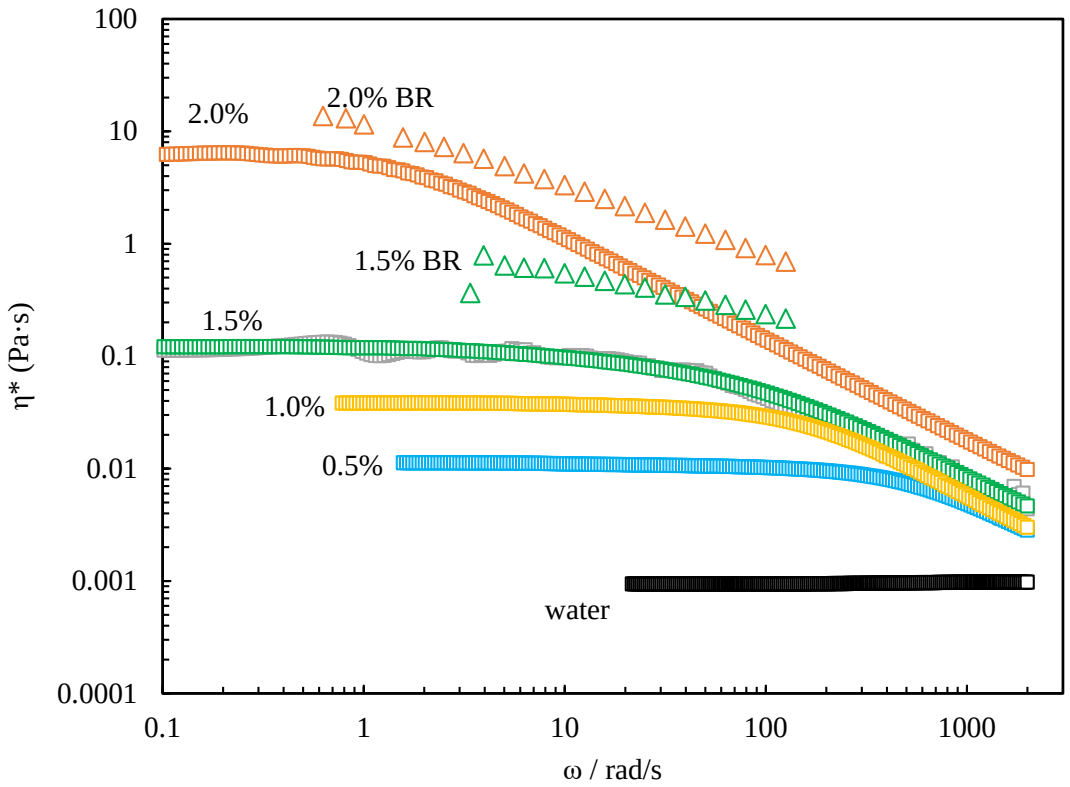

Fig. 4. Plots of complex viscosity as a function of frequency for different IC concentrations obtained by using passive microrheology (square) and bulk rheology (BR) (triangle) . The data were obtained by using the fitting function of the raw experimental data (i.e., black line for the case 1.5%).

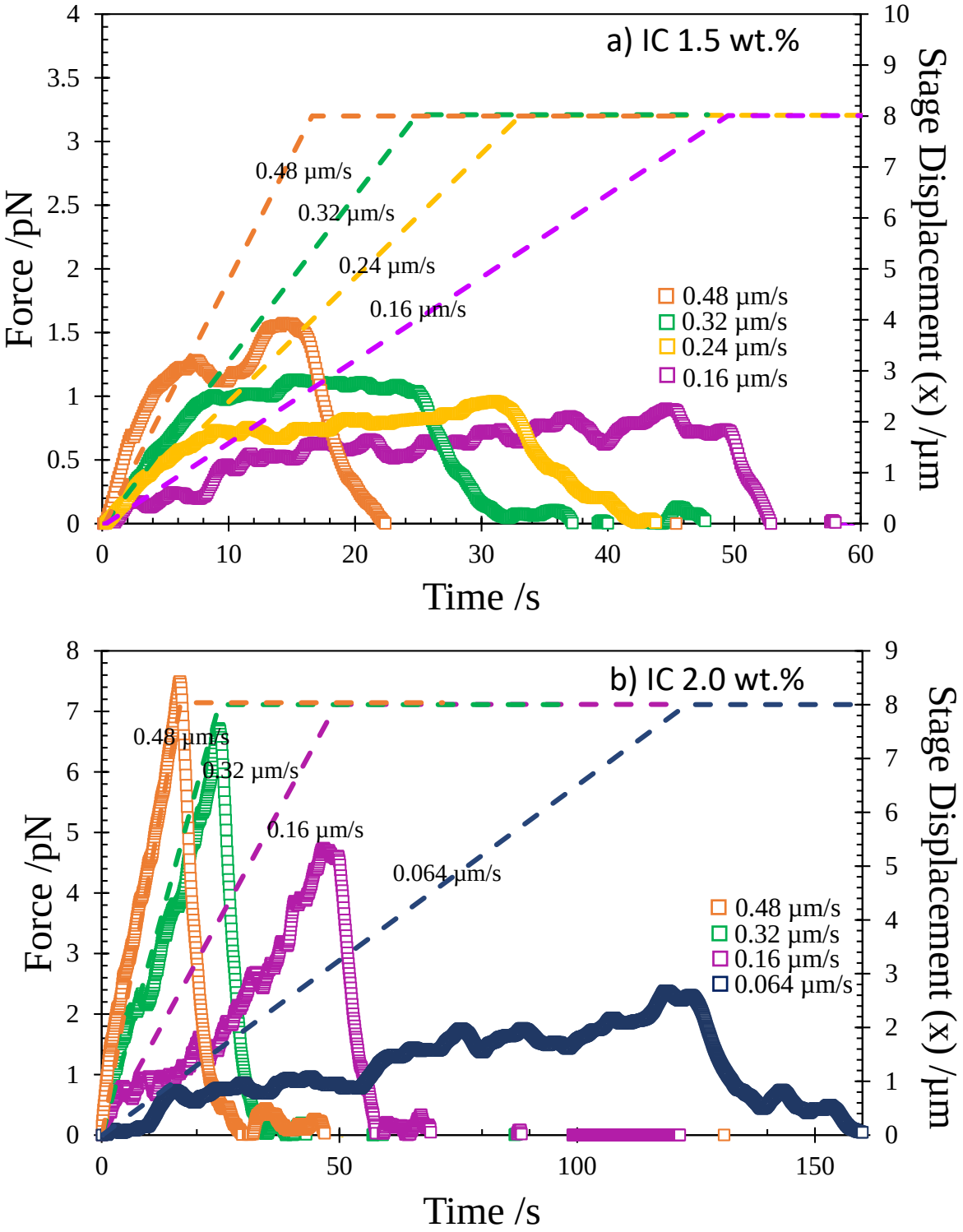

Fig. 5. Mesoscale rheology of IC gels at different strain rates using OT. The measured force response (symbols) as a function of stage movement at different speeds. The dashed line represent the stage displacement.

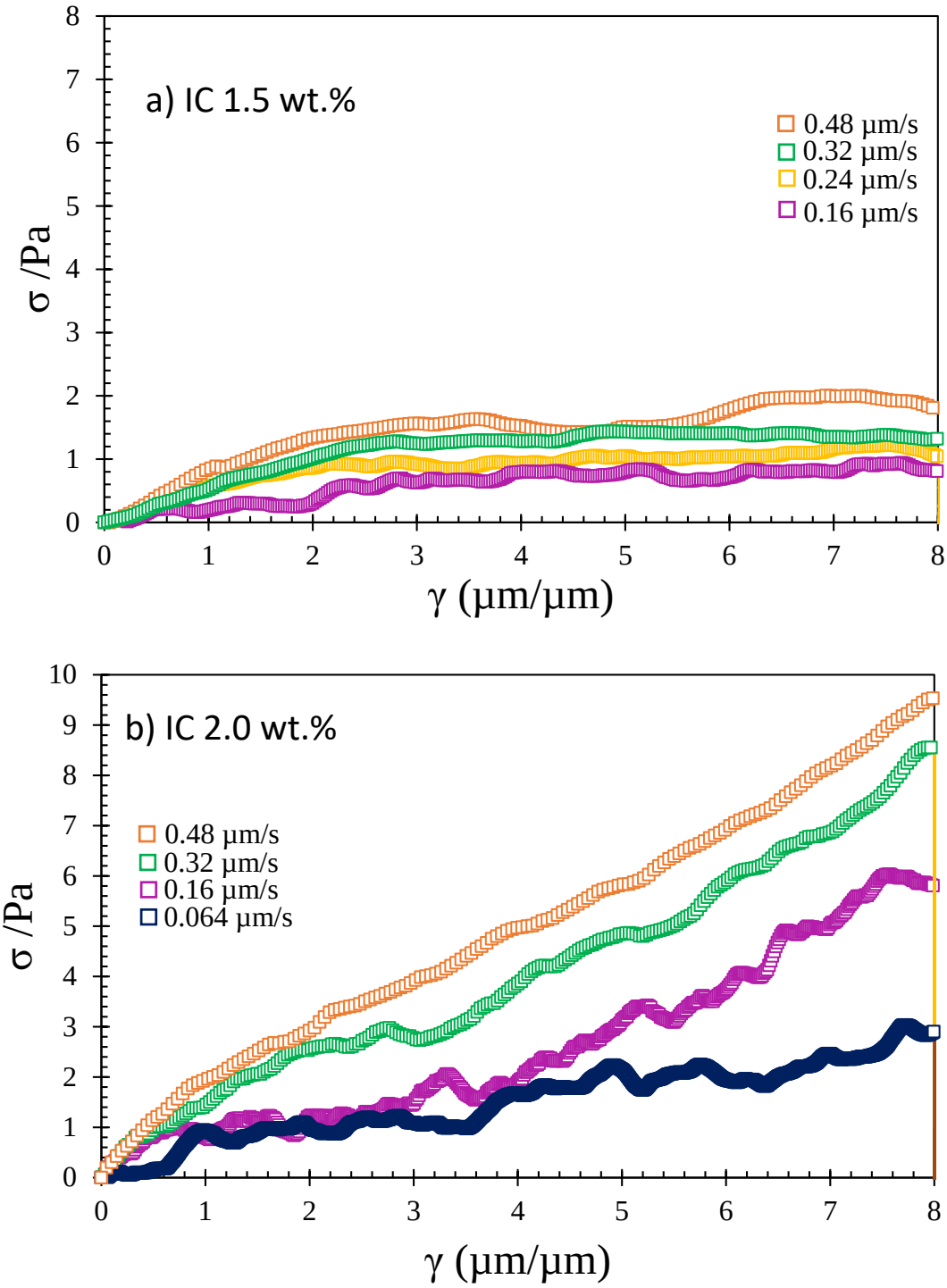

Fig. 6. Plots of σ as function γ, where $\sigma=F/\pi R^2$ and $\gamma=x/2R$, for different stage velocities.

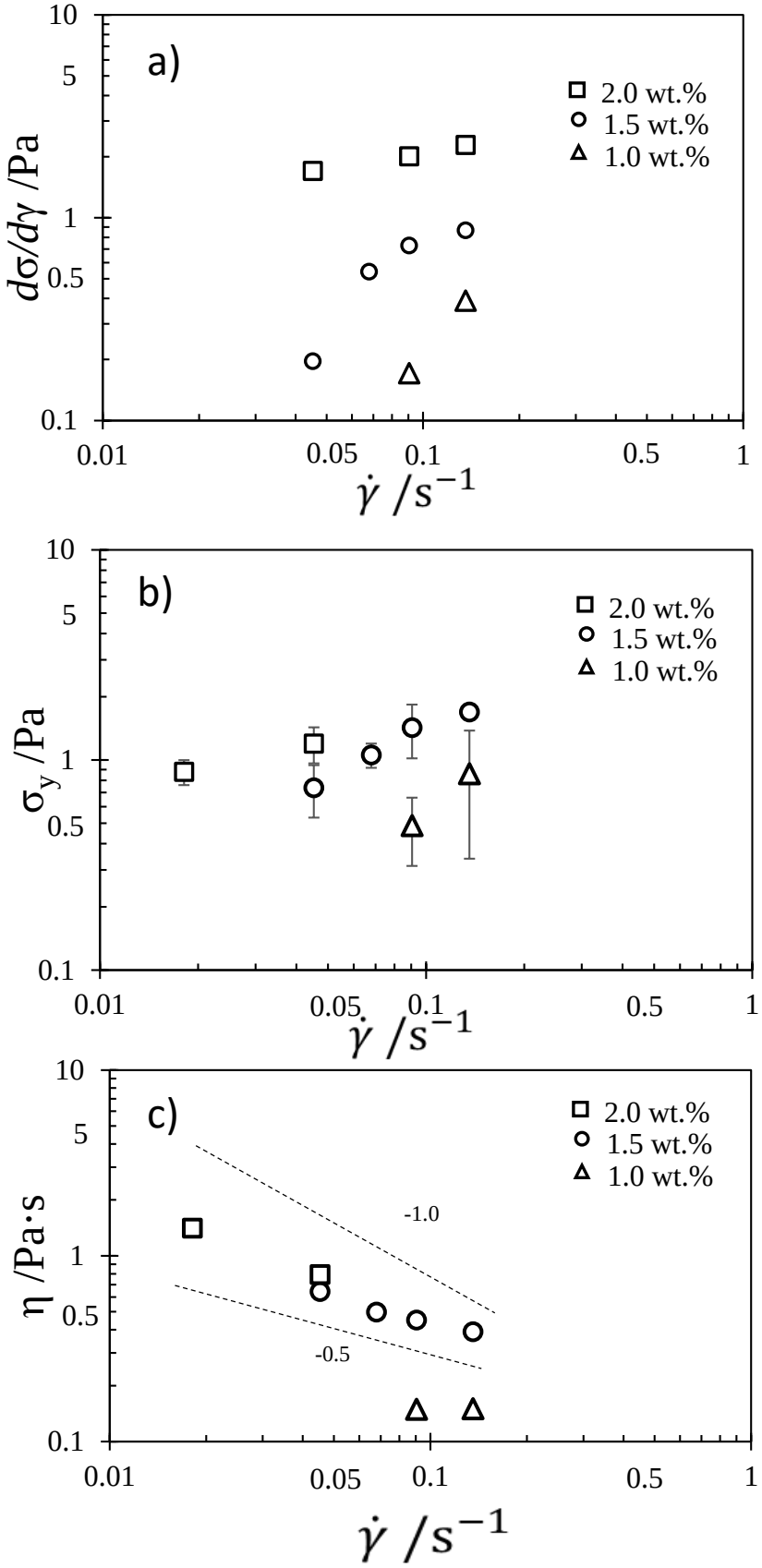

Fig. 7. Plots of the calculated rheological parameters as a function of stain rate for different IC concentrations: a) $d\sigma/d\gamma$, b) yield stress, σ_y and c) apparent viscosity η curves. A line with slope of -1 and -0.5 are drawn as guides for the gradients.

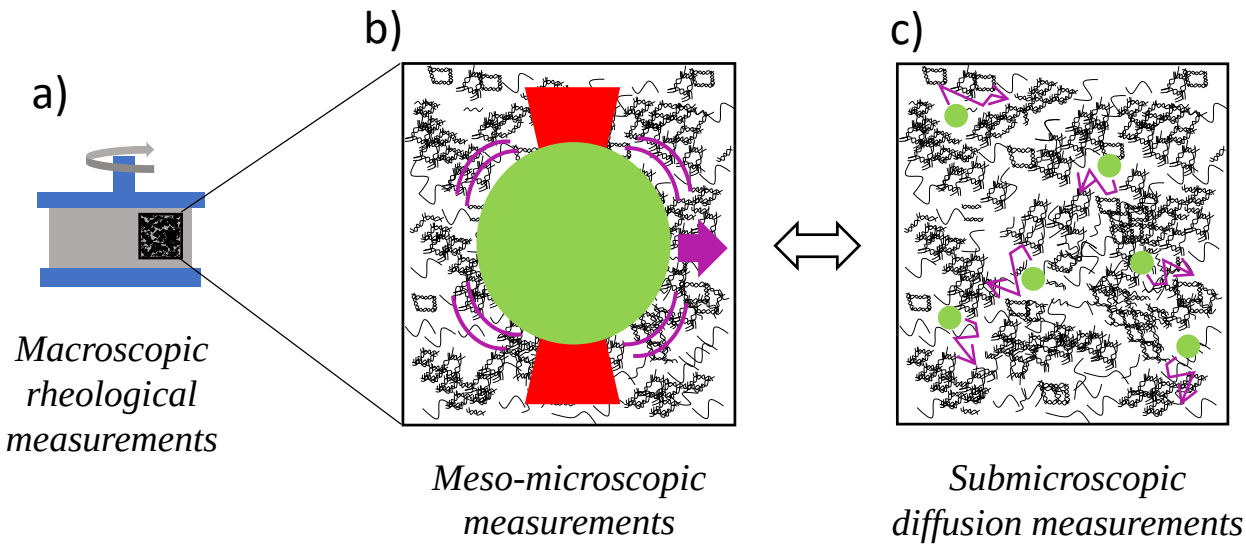

Fig. 8. Schematic representation of IC gel network developed from different investigations a) macroscopic, b) meso- to microscopic, c) submicroscopic. Figs. b-c are drawn assuming similar magnification. The arrow in the optical tweezers measurements represents the mode of deformation by the probe particle, while those in the diffusion measurements represents the thermal movement of tracer particles.

Highlights:

- Optical tweezers-based microrheology provides access to the mesoscopic properties of iota carrageenan (IC) gels
- Passive microrheology captures a wide spectral content of IC viscoelastic properties uncovering the dynamics of the network
- New insights into the hierarchical structure of IC gels were provided, especially at the mesoscopic scale

There are no conflicts of interest to declare.

Lester Geonzon: Conceptualization, Methodology, Software, Visualization, Formal Analysis, Investigation, Writing-Original Draft, Writing - Review & Editing. **Motoyoshi Kobayashi**: Supervision; Conceptualization; Methodology; Formal analysis; Validation; Visualization; Writing-original draft; Writing-review & editing; Resources; Funding acquisition; Project administration. **Manlio Tassieri:** Formal analysis; Software; Writing-review & editing. **Rommel Bacabac:** Formal Analysis; Resources; Writing - Review & Editing. **Yasuhisa Adachi**: Formal analysis; Resources; Funding acquisition; Project administration. **Shingo Matsukawa:** Formal Analysis; Resources; Writing - Review & Editing.